How to Cite: A Lobo Guerrero et al 2023 J. Phys. D: Appl. Phys. 56 065003 https://doi.org/10.1088/1361-6463/acaf8c

Crystalline texture of cobalt nanowire arrays probed by the switching field distribution and FORC diagrams

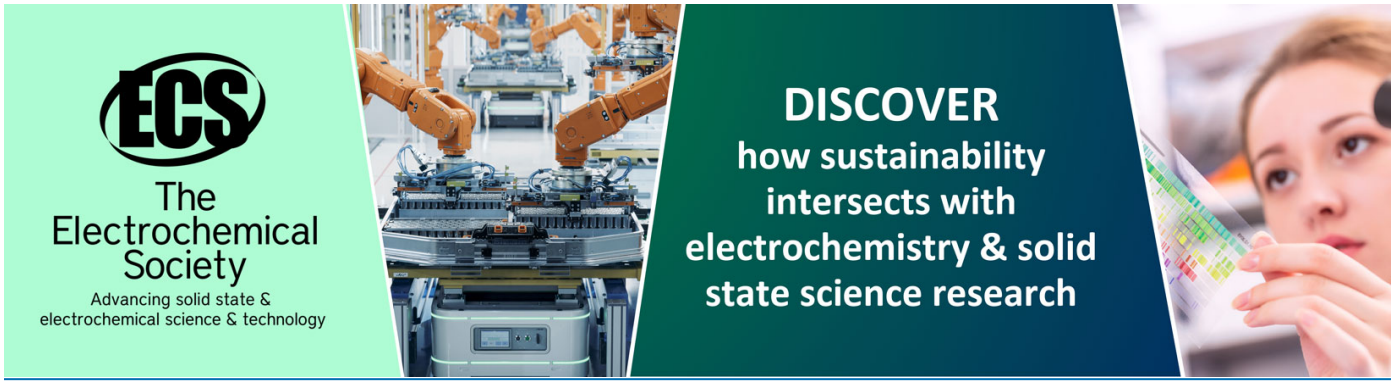

OPEN ACCESS
IOP Publishing
Journal of Physics D: Applied Physics
J. Phys. D: Appl. Phys. **56** (2023) 065003 (8pp)
https://doi.org/10.1088/1361-6463/acaf8c

Crystalline texture of cobalt nanowire arrays probed by the switching field distribution and FORC diagrams

A Lobo Guerrero[1], A Encinas[2,*], E Araujo[3], L Piraux[4] and J de la Torre Medina[5]

[1] Área Académica de Ciencias de la Tierra y Materiales, Universidad Autónoma del Estado de Hidalgo, Carretera Pachuca Tulancingo km 4.5, Ciudad del Conocimiento, Mineral de la Reforma, Hidalgo, Mexico
[2] División de Materiales Avanzados, Instituto Potosino de Investigación Científica y Tecnológica A. C., Camino a la Presa 2055, 78216 San Luis Potosí, SLP, Mexico
[3] Departamento de Matemáticas y Física, Instituto Tecnológico y de Estudios Superiores de Occidente, Periférico Sur Manuel Gómez Morín 8585, 45604 Tlaquepaque, Jalisco, Mexico
[4] Institute of Condensed Matter and Nanosciences, Université Catholique de Louvain, Place Croix du Sud 1, Louvain-la-Neuve, B-1348, Belgium
[5] Instituto de Investigaciones en Materiales—Unidad Morelia, Universidad Nacional Autónoma de México, Antigua Carretera a Pátzcuaro No. 8701 Col. Ex Hacienda de San José de la Huerta, C. P. 58190 Morelia, Mexico

E-mail: armando.encinas@gmail.com

Received 22 June 2022, revised 21 December 2022
Accepted for publication 3 January 2023
Published 20 January 2023

Abstract

The crystalline texture of arrays of low diameter Co nanowires (NWs) synthesized by electrodeposition using electrolytes with different acidities (pH in the range 2.0–6.6) was studied by the switching field distribution (SFD) and first order reversal curve (FORC) diagrams. Particularly, the SFD determined as the derivative dM/dH of the descending part of the major hysteresis loop has proven to be a reliable and powerful method for the identification of different crystalline textures in the NWs and the quantification of their corresponding texture percentages. The presence of the face centered cubic-like texture at low pH values and hexagonal close packed textures with the *c*-axis perpendicular and parallel to the NWs axis at higher pH values have been identified by performing multiple Gaussian fits to the SFD by virtue of their different magnetic behavior observed during reversal of the magnetization. The field position and size of each curve in the multiple Gaussian fit provide information about the corresponding magnetic contribution and volumetric texture percentage of each crystalline texture in the NWs, respectively. The analysis of the SFD has been complemented and validated with FORC diagram measurements, showing that the width of the coercive field distribution is in good agreement with the width of the SFD. Also, it has been found that the different branches observed in the FORC diagrams along the interaction axis provide further insight on the interaction between magnetocrystalline fields. This work provides a novel methodology for the use of magnetometry as a reliable technique for the study of the interplay between the microstructure and magnetic behavior of arrays of NWs.

Keywords: Co nanowires, switching field distribution, hysteresis loops, FORC diagrams

(Some figures may appear in colour only in the online journal)

* Author to whom any correspondence should be addressed.

1. Introduction

Arrays of very long and parallel magnetic nanowires (NWs) are interesting systems due to their particular geometry, shape anisotropy and the possibility to induce other magnetic effects of magnetocrystalline (MC) or magnetoelastic nature. Particularly, the combination of these properties make Co NWs good candidates for microwave and high density recording media applications [1]. Contrary to Ni, Fe and alloyed NWs, it is well known that electrodeposited Co NWs can exhibit the hexagonal close packed (hcp) crystalline texture, responsible for the appearance of an additional MC anisotropy contribution that superposes to the magnetostatic (MS) contribution. Indeed, the hcp texture of Co NWs can be tailored by controlling electrochemical parameters like the electrolytic bath acidity [2–6], temperature [7, 8], current density [9], deposition potential [10, 11], boric acid concentration [6], or geometrical parameters of the NWs like their diameter [12, 13], and aspect ratio [14, 15]. Furthermore, previous works have shown that Co NWs synthesized using electrolytes with pH values in the range 2.0–2.6 have preferred face centered cubic (fcc)-like texture without any MC anisotropy contribution, whereas they present the hcp texture when they are electrodeposited using electrolytes with pH values between 3.5 and 6.6. As also shown, in this pH range the orientation of the hcp *c*-axis can be either perpendicular (pH between $3.5 \lesssim \text{pH} \lesssim 5.5$) or parallel ($\text{pH} \gtrsim 6.0$) to the NWs axis [16, 17]. Nevertheless, low diameter Co NWs with mixed crystalline textures can be synthesized using electrolytes with intermediate pH values [16, 18]. The coexistence of two or three crystalline textures in the NWs modifies the way an array is magnetized, since each texture has its own magnetic behavior. Indeed, previous works on arrays Co NWs electrodeposited into porous polycarbonate (PC) [16] and alumina membranes [19] suggest a strong dependence of the magnetic and microstructural properties with the hcp *c*-axis orientation. The effective magnetic response is then expected to depend on the proportion of each textured phase present in the NWs. Previous works have reported on the identification of the different crystalline textures using ferromagnetic resonance and first order reversal curve (FORC) distributions [16, 20–22]. However, these methods are time consuming as they require recording an important amount of FORCs or absorption spectra along with significant data processing. Therefore, an easy and reliable method based on a single magnetic measurement to identify crystalline textures present in the NWs is of paramount importance. In this work, a simple protocol based on the switching field distribution (SFD) is proposed to evaluate the proportion of fcc-like and hcp crystalline textures present in arrays of low diameter Co NWs with low dipolar interaction and synthesized from electrolytes of different acidities. The analysis carried out using this protocol has been compared with the corresponding FORC diagrams. Despite the ability of FORC diagrams to detect subtle and complex magnetization processes, the SFD method has proven to provide valuable information equivalent to that of the FORC coercive field distribution (CFD) in a very simple way from single magnetization curves.

2. Experimental

2.1. Samples preparation

Arrays of 10 μm long Co NWs have been fabricated by a standard three-probe electrodeposition technique into 22 μm thick track-etched PC membranes with 45 ± 5 nm pore diameter. The length of the NWs has been estimated from the electrodeposition time required to fill the porous membranes to 45%. These PC membranes have pores density equal to 5×10^9 pores cm^2 corresponding to a porosity of 3.5%. Prior to the electrodeposition, a Cr(20 nm)/Au(600 nm) cathode was evaporated onto one side of the membrane. Cobalt NWs were grown at room temperature using 238.48 g l^{-1} $CoSO_4$ + 30 g l^{-1} H_3BO_3 electrolytes with different acidities and at a constant potential of -0.95 V versus Ag/AgCl. The electrodeposited NWs are almost perfectly cylindrical and parallel with a deviation less than 5° and have a very low surface roughness. The as-prepared solutions have a typical pH value of about 3.8, which was lowered down to 2.0 by adding dilute H_2SO_4 and increased up to 6.6 by adding 0.1 M NaOH. The electrolyte pH and magnetic parameters for all the samples considered in this work are shown in table 1.

2.2. Microstructural characterization of Co NWs

The morphology of Co NWs has been analyzed by scanning electron microscopy (SEM) using a dual beam (FIB/SEM) FEI-Helios Nanolab 600 microscope, after dissolution of the PC membrane in dichloromethane. Figure 1(a) shows a SEM micrograph displaying a bunch of broken NWs with approximate length of 4–5 μm. This micrograph confirms the cylindrical shape and high homogeneity of the NWs. The close-up view in the inset of this figure shows sharp details of the NWs, confirming a low surface roughness and the breakpoint at the tip of a NW. The crystalline orientation of Co NWs electrodeposited using electrolytes with different pH values has been evaluated by x-ray diffraction (XRD) experiments using a RIGAKU SmartLab spectrometer with Cu K_α radiation. Prior to the XRD measurements, the Cr/Au cathode was etched using a I2:KI (0.1:0.6 M) solution in order to eliminate undesired diffraction peaks arising from other elements than Co. Figure 1(b) shows the XRD patterns for arrays of electrodeposited Co NWs at pH values of 2.6, 4.4 and 6.6. As seen, the XRD pattern of the Co pH 2.6 NW array shows a main peak corresponding to the Co plane (111), which confirms their fcc structure [5]. At the intermediate pH value of 4.4, the NWs have preferential hcp crystalline texture as confirmed by the presence of the two peaks corresponding to the hcp planes (100) and (101), which is in good agreement with previous works [16, 23]. In this case, the dominant plane (100) indicates that the hcp *c*-axis is close to the direction perpendicular to the NWs. The peak corresponding to this plane disappears for the

Table 1. Coercive field (H_c) and remanence magnetization (M_r) determined by hysteresis loop measurements for Co NW arrays fabricated using electrolytes with different pH values. The number of adjusted Gaussians to the SFD is shown for comparison.

Sample	pH	H_c (kOe)	M_r (%)	Adj. Gauss.
1	2.00	1.880	98.9	1
2	2.40	1.622	98.6	2
3	2.60	1.543	96.7	2
4	3.27	1.272	92.8	2
5	3.38	1.223	88.9	2
6	3.50	1.160	84.7	2
7	3.78	1.054	75.7	2
8	3.96	1.140	71.0	2
9	4.20	1.370	76.5	2
10	4.40	1.246	91.0	2
11	4.60	1.113	76.2	2
12	4.80	1.030	71.6	2
13	5.00	1.118	68.6	2
14	5.40	1.323	64.5	3
15	5.60	1.456	66.2	3
16	5.80	1.496	72.3	3
17	6.20	2.173	95.2	2
18	6.40	2.170	98.0	2
19	6.60	2.210	99.4	1

pH 6.6 NW array for which the main diffraction is observed for the (001) plane. This result is consistent with a change of the crystal orientation of the hcp c-axis from perpendicular to parallel to the NWs axis. These microstructural changes with the pH are consistent and in good agreement with previous reports [16].

2.3. Crystalline texture evaluated using the SFD method

The SFD, also called differential susceptibility, is an important micromagnetic curve in magnetic recording media research used to evaluate the field width in which magnetization reversal takes place [24, 25]. The SFD is obtained as the derivative dM/dH of the descending branch of the major hysteresis loop (MHL) recorded by applying the magnetic field along the NWs axis direction [26, 27]. Figure 2 shows a comparison between SFD and the descending branch of the MHL for two arrays of Co NWs deposited using electrolytes with pH 2.0 (Sample 1) and 4.4 (Sample 10). As seen, the SFD for Sample 1 is symmetrical with a single peak centered around its corresponding coercive field. Conversely, the SFD for Sample 10 displays a shoulder at lower field values and its maximum is not centered at the coercive field of its MHL. As shown previously, the microstructure of Co NWs is composed of one or more crystalline textures, namely fcc-like and hcp [16, 18], where the former (later) is more likely in NWs grown using more acid (alkaline) electrolytes. The Co hcp texture is such that the c-axis can be oriented parallel ($||$) and perpendicular ($\perp$) to the NWs, then having two different hcp textures, namely hereafter $\text{hcp}_{||}$ and $\text{hcp}_{\perp}$. Co NWs grown using electrolytes with intermediate acidities have a combination of

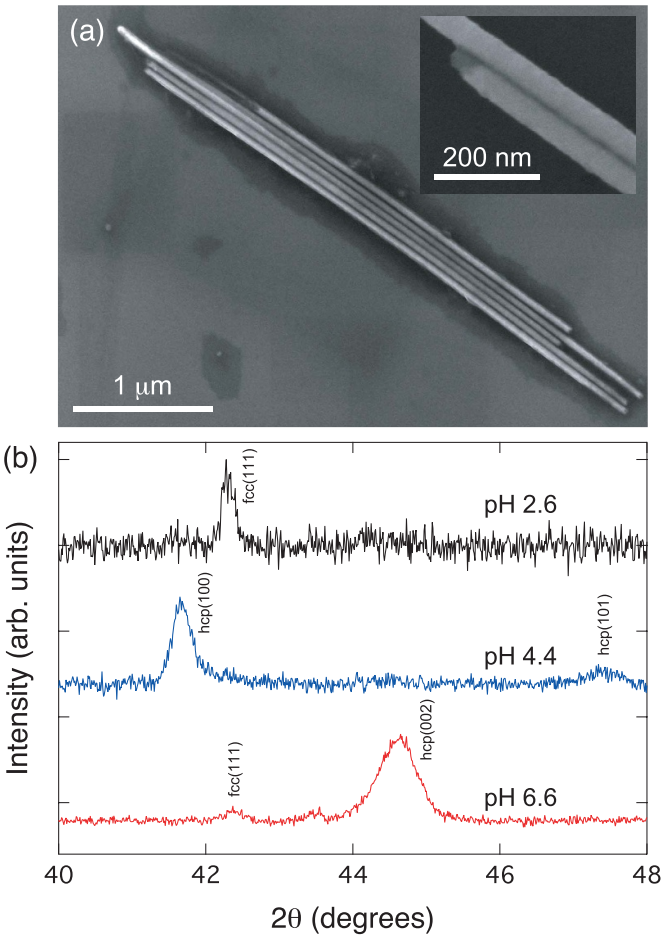

Figure 1. (a) SEM micrograph of Co NWs after dissolution of the PC membrane. The inset shows a close view of two NWs with average diameter of 45 ± 5 nm. (b) XRD patterns for arrays of Co NWs electrodeposited using electrolytes at the pH values of 2.6, 4.4, and 6.6.

these textures, each one behaving as a well-defined magnetic phase with specific coercivity, resulted from the superposition of their MC and MS anisotropies. As a consequence, the SFD can exhibit various peaks, each one associated to a different crystalline texture. To evaluate the presence of these crystalline textures, a numerical fit based on the superposition of one to three Gaussian curves is performed to the experimental SFD. In this context, two conditions must be met for optimal Gaussian-based curve fitting: (a) the coercive fields of single phases (or textures) must be different to prevent overlapping, and (b) the volume of secondary phases must be large enough to be measured. Both conditions are necessary to be able to distinguish between the different contributions in the SFD, otherwise a single and wider peak will be observed.

2.4. Crystalline texture evaluated using FORC diagrams

The FORC distribution $\rho(H, H_r)$ is defined as the mixed second derivative of a series of FORCs ($M(H, H_r)$ curves) with respect to H_r and H, that is [28]

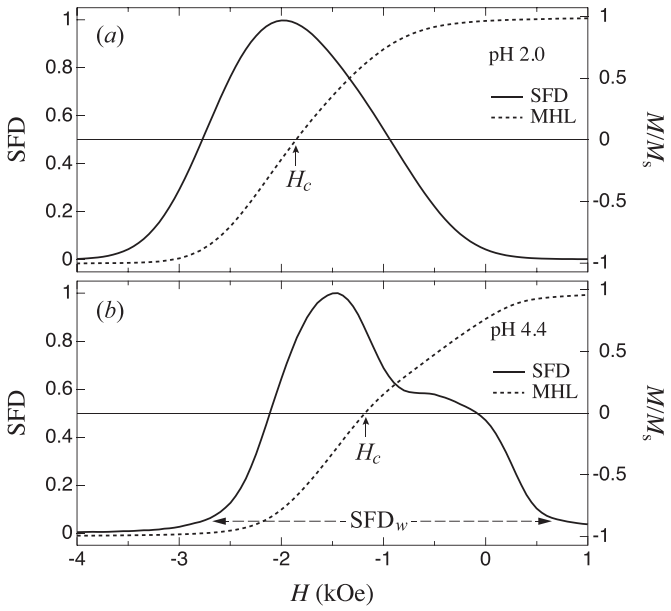

Figure 2. Switching field distribution (continuous line) obtained from the descending branch of the MHL (dotted line) for the Co NW arrays with (a) pH = 2.0 (Sample 1) and (b) pH = 4.4 (sample 10) (see table 1).

$$\rho(H,H_r) = -\frac{1}{2}\frac{\partial^2 M(H,H_r)}{\partial H_r \partial H}. \quad (1)$$

Then, a new set of coordinates defined as $H_c = (H_r - H)/2$ and $H_u = (H_r + H)/2$ is used to rotate the FORC distribution by 45° counterclockwise. The new coordinates H_c and H_u provide information about the mean coercivity and interaction of individual NWs with the surrounding NW array, respectively [20]. The final FORC diagram is a contour plot of $\rho(H_r,H)$, with H_c and H_u on the horizontal and vertical axes, respectively [29–31]. For each sample, 200 FORCs were measured and used along with the FORCinel 2.0 software [31] to generate FORC diagrams with very high resolution. The analysis of FORC diagrams has been performed in terms of the CFD and the interaction field distribution (IFD) along the H_c and H_u axes, respectively.

3. Results and discussion

3.1. Co NWs with single crystalline texture

Arrays of Co NWs with single texture are either polycrystalline fcc-like or have preferential $hcp_{||}$ crystal orientation with the *c*-axis along the NWs axis. The former (later) has been obtained using an electrolyte with its pH adjusted to 2.0 (6.6). As seen in figures 3(a) and (q) the SFD for these two NW arrays shows a single peak, which is consistent with the presence of a single magnetic phase; as will be further evidenced by the results of the intermediate pH cases. However, the single peaks for the fcc-like and $hcp_{||}$ NW arrays are centered in 1.88 kOe and 2.21 kOe, respectively. The larger center field for the NW with $hcp_{||}$ texture is associated to the magnetic anisotropy. As known, the anisotropy field for arrays

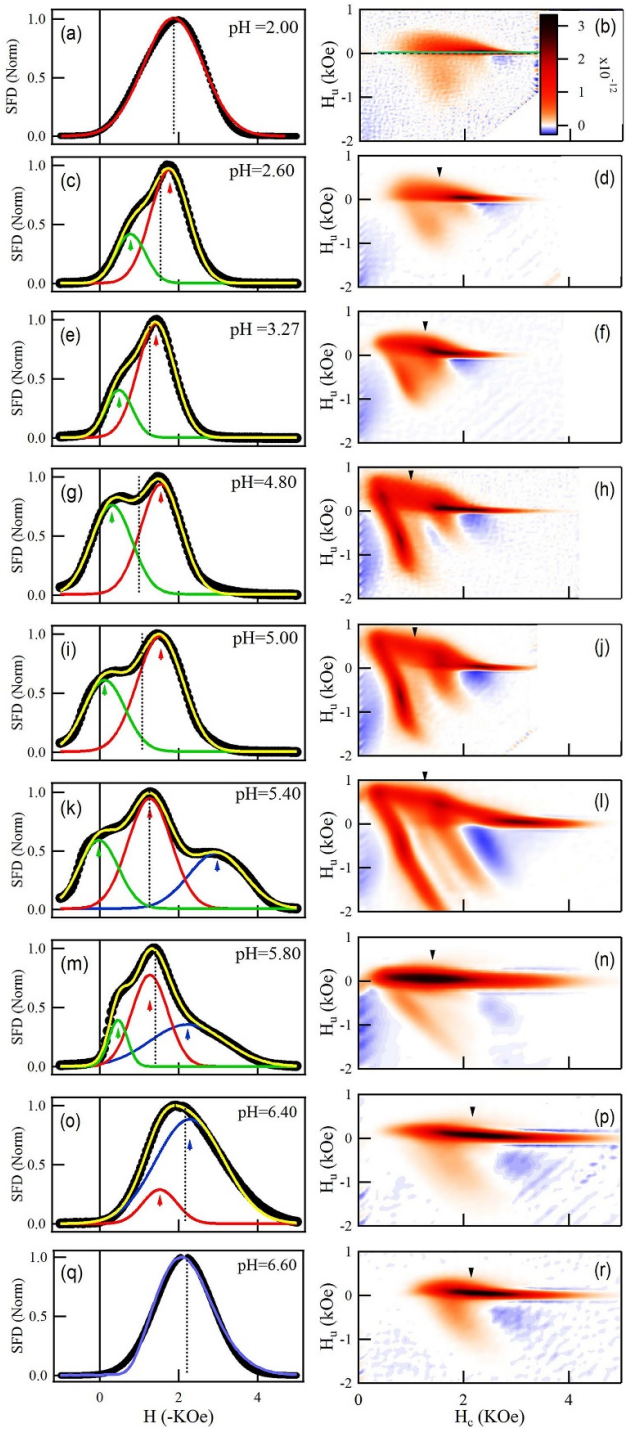

Figure 3. (left) Experimental SFD curves (•) and effective Gaussian fit (yellow line) resulted from the sum of individual Gaussian fits for the fcc-like (red line), $hcp_{\perp}$ (green line) and $hcp_{||}$ (blue line) crystalline textures. The dotted line indicates the coercive field of each NW array. (right) FORC diagrams plotted in the H_u–H_c plane, where the black triangle (▼) on top of each diagram indicates the position of the coercive field.

of $hcp_{||}$ Co NWs is the result of the superposition of the MS and MC contributions, which is larger than the anisotropy field for arrays of fcc-like Co NWs because it corresponds only to the MS contribution [16]. These single-textured NW arrays are of particular importance as they serve as reference systems to

study the magnetic behavior and microstructure of NW arrays with mixed crystalline textures. On the other hand, the FORC diagram for the fcc-like Co NWs is characteristic of a low interaction system, as indicated by the narrow width Δ_{IFD} of the IFD along the H_{u} axis. This result is consistent with the expected low MS interactions due to the low packing fraction of the NW arrays studied in this work.

Besides, the FORC diagram for the $\mathrm{hcp}_{||}$ NW array in figure 3(r) shows that MS interactions remain low, as expected because all NW arrays studied in this work have the same packing fraction. Magnetization reversal, on the other hand, takes place in a CFD centered at a higher field than that of the fcc-like NW array (see the triangles on top of figures 3(b) and (r)). This result is in good agreement with that obtained with the SFD.

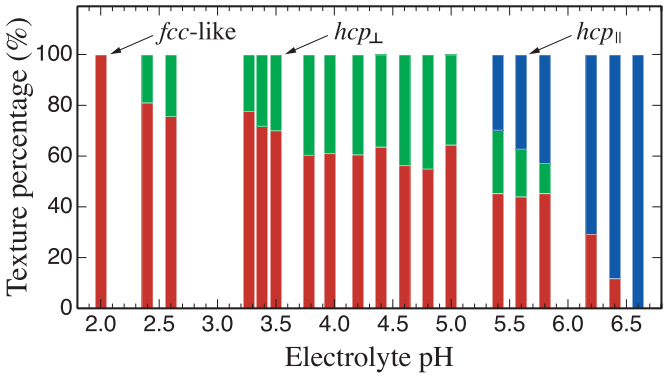

Figure 4. Crystalline texture percentages of Co NW arrays as a function of the electrolyte pH, determined from the area below each curve of the multiple Gaussian fit to the SFD.

3.2. Co-NWs with multiple crystalline textures

In contrast to Co NWs with single crystalline texture obtained at pH values of 2.0 and 6.6, previous works show that arrays of Co NWs synthesized using electrolytes with intermediate pH values have a combination of crystalline textures. Specifically, FMR experiments have shown that Co NW arrays synthesized from electrolytes with pH values between 2.0 and 6.6 have a magnetic anisotropy lower than those for the fcc-like and $\mathrm{hcp}_{||}$ phases [16]. It has also shown that the dominant microstructure of these NWs has texture $\mathrm{hcp}_{\perp}$ with the *c*-axis oriented perpendicular to the NWs axis. Therefore, the average microstructure of Co NWs can vary from a fcc-like structure with no MC anisotropy at low pH, to a textured polycrystalline hcp structure with the *c*-axis perpendicular to the NWs axis at intermediate pH values (3–5.5) and with the *c*-axis parallel to the NWs at higher pH values (5.5–6.6). These structural changes can be inferred from the SFD and FORC diagrams shown in figure 3. That is, arrays of Co NWs with $2.4 \leqslant \mathrm{pH} \leqslant 5.0$ (Samples 2–13) have a combination of fcc-like and $\mathrm{hcp}_{\perp}$ crystalline textures, as suggested by the SFD line-shape displaying either two peaks or a single peak with a shoulder at lower field values. Clearly, the curves line-shape can be well reproduced using a two-Gaussian fit, as shown in figures 3(c), (e), (g) and (i).

Besides, the effective magnetic anisotropy of the $\mathrm{hcp}_{\perp}$ crystalline texture is the result of the competition between the MC and MS contributions because they oppose each other. That is, the MS field constrains the magnetization along the NWs axis, while the MC field constrains the magnetization in the direction perpendicular to the NWs axis. As a result of this competition, the MC field is subtracted from the MS field and the effective anisotropy for the $\mathrm{hcp}_{\perp}$ texture is lower than the MS contribution alone which is characteristic of the fcc-like texture. Therefore, for these NW arrays the peak centered at higher ($\approx$1.5 kOe) and lower ($\approx$0.84 kOe) fields corresponds to the fcc-like and $\mathrm{hcp}_{\perp}$ textures, respectively. The Gaussian fits associated with the fcc-like texture (red curves) maintain their field position and shape as the pH increases, while those associated with the $\mathrm{hcp}_{\perp}$ texture (green curves) increase in height and width, reaching their maximum at $\mathrm{pH} = 4.80$. This behavior is consistent with an increase of the $\mathrm{hcp}_{\perp}$ texture with the pH, which can be quantified from the shape and size of each individual Gaussian fit. Indeed, these parameters are directly related to the area below each Gaussian fit, which can be used as a measure of the percentage of its corresponding crystalline texture. Therefore, the total texture of the NWs reflects the contribution and weighted importance of the different textures, as shown in figure 4. This figure shows that the $\mathrm{hcp}_{\perp}$ texture increases with the pH at the expense of the reduction of the fcc-like texture.

Furthermore, the FORC diagrams of Samples 2 to 13 show an increase of Δ_{CFD} in the range between 2.6 and 3.3 kOe, which is in good agreement with the increase in width of their corresponding SFD (see figures 3(d)–(j)). Besides, the width Δ_{IFD} of the IFD for these NW arrays increases from 1.7 to 2.7 kOe as the pH increases. This interaction field is clearly different from the MS dipolar interaction field. This is because the later is constant as it depends on their packing fraction, which is the same for all the NW arrays in this study. Contrary to the IFD for Sample 1 observed in figure 3(b), the IFD for Samples 2–13 in figures 3(d)–(j) show two well visible curved branches (red to black shadow zones) along the H_{u} axis. Each IFD branch is associated to a different crystalline structure according to its corresponding mean coercive field, where the wider (narrower) branch at lower (higher) coercive fields correspond to the $\mathrm{hcp}_{\perp}$ (fcc-like) texture. Therefore, each branch provides information about the interaction field experienced by each crystalline texture in an individual NW due to the entire NW array. The larger Δ_{IFD} observed for the lower field branch is consistent with the fact that the large MC contribution due to the $\mathrm{hcp}_{\perp}$ texture favors an easy magnetization plane perpendicular to the NWs axis that reinforces interactions between them and helps magnetization reversal to occur faster.

As the pH is further increased in the range 5.4–5.8 (Samples 14, 15 and 16), the SFD displays three peaks as a result of multiple mixed crystalline textures (see figures 3(k) and (m)). The two Gaussians at low fields (green and red curves) in the multiple Gaussian fit correspond to the $\mathrm{hcp}_{\perp}$ and fcc-like crystalline textures, as expected, but the third one at higher fields (blue curve) is consistent with the presence of the $\mathrm{hcp}_{||}$ crystalline texture. Indeed, the Gaussian peak at 2.1 kOe for

this texture is proportional to the largest effective magnetic anisotropy of Co NWs that results from the superposition of their MC and MS fields [16]. In this pH range, the Gaussian amplitude for the fcc-like texture still dominates over the hcp texture. However, the $hcp_{||}$ texture grows at the expense of the $hcp_{\perp}$ texture because the fcc-like texture percentage remains almost unchanged, as seen in figure 4. This result is in good agreement with the NWs growth mechanism discussed above in which a polycrystalline segment grows at the initial growth stage [32]. As seen in figure 3(l), the FORC diagram of Sample 14 shows the widest CFD, in agreement with its SFD showing three peaks with high deconvolution (see figure 3(k)). These three peaks are reflected in the IFD as three branches along the H_u axis, with the one at middle H_c values a little less visible than the other two. As comparing the FORC diagrams in figure 3, the branches for this sample extended along the H_u axis are the longest ones, indicating a very strong interaction for the $hcp_{\perp}$ crystalline texture. This result shows that the larger this interaction, the lower the remanence magnetization M_r, as corroborated by the corresponding value for Sample 14 in table 1, since it is the lowest M_r value of all the samples in this study.

As the pH increases further between 6.2 and 6.4 (see Samples 17 and 18), the SFD consists in a single broad peak which is better reproduced by a two Gaussian fit, as seen in figure 3(o). These Gaussians observed at high and middle coercive fields are consistent with the presence of a dominant $hcp_{||}$ and a small amount of fcc-like crystalline textures, respectively. The $hcp_{\perp}$ texture has vanished for these samples due to the absence of the Gaussian peak at low field values. Indeed, previous works have shown that Co NWs synthesized at pH values above 5.4 are mainly single crystalline with the hcp *c*-axis oriented along the NWs axis [16]. Despite of the absence of the $hcp_{\perp}$ texture for these samples, $\Delta_{CFD} \approx 3.1$–4.9 kOe remains almost unchanged from the value of samples 14, 15, and 16. This large Δ_{CFD} value for Samples 14–18 can be ascribed to the dominant hcp texture (see figure 4) and reflects the large dispersion of the MC anisotropy. Concerning the IFD for Samples 17 and 18 with dominant $hcp_{||}$ texture, it shows a single branch along the H_u axis with $\Delta_{IFD} \approx 1.2$ kOe. This feature is due to the absence of the $hcp_{\perp}$ texture and the presence of a very low fcc-like texture percentage, where this later is yet present because of its preferential growth in the early stage of the NWs electrodeposition process [13]. A previous work suggests that a pH gradient is induced within the nanopores, such that an acidic environment is produced at the bottom of the nanopores, which favors the formation of the fcc-like texture [33]. As the NWs growth continues above the middle of the nanopores, the pH within them increases and the formation of the $hcp_{\perp}$ texture is promoted. Therefore, depending on the pH of the bulk electrolyte outside the nanopores, the growth of $hcp_{||}$ texture can be promoted if the electrolyte is sufficiently alkaline. Therefore, the growth of the $hcp_{||}$ texture can be promoted if the electrolyte is sufficiently alkaline in order to counteract the pH gradient established within the nanopores. This means that for electrolyte pH values close to 6.6, an earlier $hcp_{||}$ growth is preferred, replacing the $hcp_{\perp}$ growth and hindering or even replacing the initial polycrystalline stage.

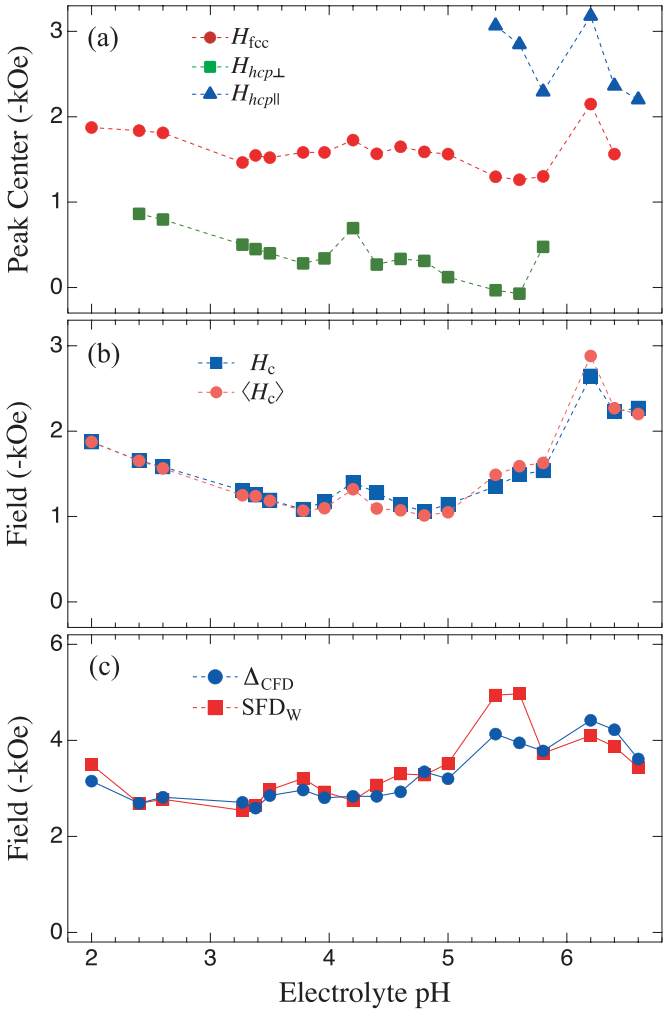

Figure 5. (a) Variation of the fields at peaks centers H_{fcc}, $H_{hcp\perp}$, and $H_{hcp||}$ from individual Gaussian fits corresponding to the fcc-like (circles), $hcp_{\perp}$ (squares) and $hcp_{||}$ (triangles) crystalline textures. (b) Coercive field H_c measured from the MHL (squares) compared with the average coercive field $\langle H_c \rangle$ (circles) calculated using equation (2). (c) Comparison between the full width of the FORC-CFD Δ_{CFD} (circles), and the full width of the SFD obtained from the MHL (squares).

3.3. *Contribution of crystalline textures to the coercive field*

Figure 5(a) shows the variations of the field value at peak center vs. pH obtained from the Gaussian fits for each texture, which are denoted as H_i for $i =$ fcc, $hcp_{\perp}$, $hcp_{||}$. Particularly, H_{fcc} remains nearly constant and lies in intermediate field values, whereas $H_{hcp\perp}$ lies in lower field values and decreases as the pH increases, corroborating the competition between the MS and MC fields and the enhancement of the latter through the increase of its corresponding texture percentage (see figure 4). Conversely, $H_{hcp||}$ lies at higher fields than H_{fcc} and $H_{hcp\perp}$, which is consistent with the superposition between the MS and MC anisotropies. The coercive field (H_c) of the

MHL shown in figure 5(b) is the result of the magnetic contributions from the distinct crystalline phases present in each NW array. To corroborate this assumption consider that the coercive field is the weighted average of the peak center fields (H_i) contributing to each array, that is

$$\langle H_c \rangle = \sum_i T_i H_i, \tag{2}$$

where $T_i = A_i/A_{SFD}$ with $i =$ fcc, hcp$_\perp$, hcp$_{||}$ is the texture coefficient defined as the quotient between the area below the Gaussian fit (A_i) and the area below the SFD (A_{SFD}). These texture coefficients correspond to the texture percentages given in figure 4, so only those contributing to the total NWs texture must be considered in the calculation of $\langle H_c \rangle$ using equation (2). The very good agreement between the variation of H_c and $\langle H_c \rangle$ vs pH observed in figure 5(b) validates equation (2) and thus corroborates the assumption that H_c is the average of the H_i fields. However, as pointed out by equation (2), each field must be weighted by its corresponding texture percentage present in the NWs. Validation of this equation provides a methodology for the determination of unknown crystalline texture percentages as long as the others are well known. Besides, the width of the SFD (SFD$_w$) provides further information about the magnetic behavior of each crystalline texture, since its observed increase in figure 5(c) shows that the magnetic anisotropy for the hcp texture is more dispersed than the one for the fcc-like texture. That is, the larger SFD$_w$ values observed at pH $\geqslant$ 5.4 are due to the dominant hcp texture, consistent with what is observed in figure 3 for larger Δ_{CFD} values at larger pH values. As seen in figure 5(c), the good agreement between the variation of both SFD$_w$ and Δ_{CFD} means that the SFD provides the same information as the CFD shown on the FORC diagrams, which is consistent with previous results on ferromagnetic NW arrays [34].

4. Conclusion

We have shown that the SFD is a reliable and powerful method to study the relationship between the magnetic and microstructural properties of electrodeposited Co NW arrays with control on the crystalline texture by the electrolyte acidity. This method consists on the determination of the SFD from the descending part of the MHL. By performing multiple Gaussian fits to the SFD, it has been possible to identify different magnetic contributions corresponding to specific percentages of fcc-like and hcp crystalline textures, with the *c*-axis oriented perpendicular (hcp$_\perp$) and parallel (hcp$_{||}$) to the NWs axis. Specifically, this approach has permitted to distinguish between NW arrays with the fcc-like and the hcp$_{||}$ single textures at pH values of 2.0 and 6.6, respectively, and with mixed textures at intermediate pH values. By properly identifying all the different textures in the NWs, it has been shown that the coercive field can be expressed as the weighted average of their magnetic contributions. It has also shown that the SFD is equivalent and provides the same information as the FORC-CFD since they have the same full width. Then, the simplicity of the SFD in comparison with the FORC-CFD lies on its feasibility of obtaining the same information from a single and reliable measurement. Finally, this work paves the way on the use of magnetometry for the study of the interplay between the microstructure and magnetic behavior of arrays of NWs in a simple and reliable way.

Data availability statement

The data that support the findings of this study are available upon request from the authors.

Acknowledgments

The authors thank Dr Etienne Ferain from it4ip S. A. for supplying the polycarbonate membranes. This work was partly supported by CONACYT Ciencia Básica Projects 286626 and A1-S-9588, as well as the Wallonia/Brussels Community (ARC 18/23-093) and the Belgian Fund for Scientific Research (FNRS). We thank Laboratorio Nacional de Investigaciones en Nanociencias y Nanotecnologia (LINAN) IPICYT for access to their facilities as well as technical support from Dr Gladis Labrada (SEM) and M C Beatriz Rivera (XRD).

ORCID iDs

A Encinas https://orcid.org/0000-0003-4965-282X
L Piraux https://orcid.org/0000-0003-0684-4338
J de la Torre Medina https://orcid.org/0000-0002-7014-8073

References

[1] García J M, Asenjo A, Velázquez J, García D, Vázquez M, Aranda P and Ruiz-Hitzky E 1999 Magnetic behavior of an array of cobalt nanowires *J. Appl. Phys.* **85** 5480–2
[2] Encinas A, Demand M, George J-M and Piraux L 2002 Effect of the pH on the microstructure and magnetic properties of electrodeposited cobalt nanowires *IEEE Trans. Magn.* **38** 2574–6
[3] Cortés A, Lavín R, Denardin J C, Marotti R E, Dalchiele E A, Valdivia P and Gómez H 2011 Template assisted electrochemical growth of cobalt nanowires: influence of deposition conditions on structural, optical and magnetic properties *J. Nanosci. Nanotechnol.* **11** 3899–3910
[4] Vivas L G, Escrig J, Trabada D G, Badini-Confalonieri G A and Vázquez M 2012 Magnetic anisotropy in ordered textured Co nanowires *Appl. Phys. Lett.* **100** 252405
[5] Shaterabadi Z, Soltanian S, Koohbor M, Salimi A and Servati P 2015 Modification of microstructure and magnetic properties of electrodeposited Co nanowire arrays: a study of the effect of external magnetic field, electrolyte acidity and annealing process *Mater. Chem. Phys.* **160** 389–97
[6] Agarwal S and Khatri M S 2022 Effect of pH and boric acid on magnetic properties of electrodeposited Co nanowires *Proc. Natl Acad. Sci. India* A **92** 111–6
[7] Kaur D, Pandya D K and Chaudhary S 2012 Texture changes in electrodeposited cobalt nanowires with bath temperature *J. Electrochem. Soc.* **159** D713–6

[8] Han X, Liu Q, Wang J, Li S, Ren Y, Liu R and Li F 2009 Influence of crystal orientation on magnetic properties of hcp Co nanowire arrays *J. Phys. D: Appl. Phys.* **42** 095005
[9] Cho J U, Wu J-H, Min J H, Ko S P, Soh J Y, Liu Q X and Kim Y K 2006 Control of magnetic anisotropy of Co nanowires *J. Magn. Magn. Mater.* **303** e281–5
[10] Mehmood T, Shahzad Khan B, Mukhtar A, Chen X, Yi P and Tan M 2014 Mechanism for formation of fcc-cobalt nanowires in electrodeposition at ambient temperature *Mater. Lett.* **130** 256–8
[11] Wang M, Wu Z, Yang H and Liu Y 2018 Growth orientation control of Co nanowires fabricated by electrochemical deposition using porous alumina templates *Cryst. Growth Des.* **18** 479–87
[12] Maaz K, Karim S, Usman M, Mumtaz A, Liu J, Duan J L and Maqbool M 2010 Effect of crystallographic texture on magnetic characteristics of cobalt nanowires *Nanoscale Res. Lett.* **5** 1111
[13] Ali G, Ahmad M, Akhter J I, Maaz K, Karim S, Maqbool M and Yang S G 2010 Characterization of cobalt nanowires fabricated in anodic alumina template through ac electrodeposition *IEEE Trans. Nanotechnol.* **9** 223–8
[14] Kaur D, Chaudhary S and Pandya D K 2013 Manifestations in the magnetization of the *hcp*-Co nanowires due to interdependence of aspect ratio and *c*-axis orientation *J. Appl. Phys.* **114** 043909
[15] Sánchez-Barriga J, Lucas M, Radu F, Martin E, Multigner M, Marin P, Hernando A and Rivero G 2009 Interplay between the magnetic anisotropy contributions of cobalt nanowires *Phys. Rev.* B **80** 184424
[16] Darques M, Encinas A, Vila L and Piraux L 2004 Controlled changes in the microstructure and magnetic anisotropy in arrays of electrodeposited Co nanowires induced by the solution pH *J. Phys. D: Appl. Phys.* **37** 1411
[17] Darques M, Piraux L, Encinas A, Bayle-Guillemaud P, Popa A and Ebels U 2005 Electrochemical control and selection of the structural and magnetic properties of cobalt nanowires *Appl. Phys. Lett.* **86** 072508
[18] Zafar N, Shamaila S, Sharif R, Wali H, Naseem S, Riaz S and Khaleeq ur Rahman M 2015 Effects of pH on the crystallographic structure and magnetic properties of electrodeposited cobalt nanowires *J. Magn. Magn. Mater.* **377** 215–9
[19] Ivanov Y P, Vivas L G, Asenjo A, Chuvilin A, Chubykalo-fesenko O and Vázquez M 2013 Magnetic structure of a single-crystal hcp electrodeposited cobalt nanowire *Europhys. Lett.* **102** 17009
[20] Ciureanu M, Béron F, Ciureanu P, Cochrane R W, Ménard D, Sklyuyev A and Yelon A 2008 First order reversal curves (FORC) diagrams of Co nanowire arrays *J. Nanosci. Nanotechnol.* **8** 5725–32
[21] Proenca M P, Merazzo K J, Vivas L G, Leitao D C, Sousa C T, Ventura J, Araujo J P and Vazquez M 2013 Co nanostructures in ordered templates: comparative FORC analysis *Nanotechnology* **24** 475703
[22] Montazer A H, Ramazani A, Almasi Kashi M and Zavašnik J 2016 Angular-dependent magnetism in Co(001) single-crystal nanowires: capturing the vortex nucleation fields *J. Mater. Chem.* C **4** 10664–74
[23] Schlörb H, Haehnel V, Khatri M S, Srivastav A, Kumar A, Schultz L and Fähler S 2010 Magnetic nanowires by electrodeposition within templates *Phys. Status Solidi* b **247** 2364–79
[24] Sharrock M P 1989 Particulate magnetic recording media: a review *IEEE Trans. Magn.* **25** 4374–89
[25] van de Veerdonk R J M, Wu X and Weller D 2003 Determination of switching field distributions for perpendicular recording media *IEEE Trans. Magn.* **39** 590–3
[26] Berger A, Xu Y, Lengsfield B, Ikeda Y and Fullerton E E 2005 $\Delta H(M, \Delta M)$ method for the determination of intrinsic switching field distributions in perpendicular media *IEEE Trans. Magn.* **41** 3178–80
[27] Berger A, Lengsfield B and Ikeda Y 2006 Determination of intrinsic switching field distributions in perpendicular recording media (invited) *J. Appl. Phys.* **99** 08E705
[28] Pike C R 2003 First-order reversal-curve diagrams and reversible magnetization *Phys. Rev.* B **68** 104424
[29] Egli R, Chen A P, Winklhofer M, Kodama K P and Horng C-S 2010 Detection of noninteracting single domain particles using first-order reversal curve diagrams *Geochem. Geophys. Geosyst.* **11** Q01Z11
[30] Spinu L, Stancu A, Radu C, Li F and Wiley J B 2004 Method for magnetic characterization of nanowire structures *IEEE Trans. Magn.* **40** 2116–8
[31] Harrison R J and Feinberg J M 2008 FORCinel: an improved algorithm for calculating first-order reversal curve distributions using locally weighted regression smoothing *Geochem. Geophys. Geosyst.* **9** Q05016
[32] Huang X, Li L, Luo X, Zhu X and Li G 2008 Orientation-controlled synthesis and ferromagnetism of single crystalline Co nanowire arrays *J. Phys. Chem.* C **112** 1468–72
[33] Darques M, Piraux L and Encinas A 2005 Influence of the diameter and growth conditions on the magnetic properties of cobalt nanowires *IEEE Trans. Magn.* **41** 3415–7
[34] Velázquez Y G, Lobo Guerrero A, Martínez J M, Araujo E, Tabasum M R, Nysten B, Piraux L and Encinas A 2020 Relation of the average interaction field with the coercive and interaction field distributions in first order reversal curve diagrams of nanowire arrays *Sci. Rep.* **10** 21396